SCIENTIFIC REPORTS

OPEN

SUBJECT AREAS:
NANOPARTICLES
BIOMEDICAL MATERIALS

Received
17 January 2014

Accepted
7 March 2014

Published
24 March 2014

Correspondence and requests for materials should be addressed to H.F.C. (haifeng.chen@pku.edu.cn)

Investigation on the structure and upconversion fluorescence of Yb^{3+}/Ho^{3+} co-doped fluorapatite crystals for potential biomedical applications

Xiyu Li[1], Jingxian Zhu[2], Zhentao Man[2], Yingfang Ao[2] & Haifeng Chen[1]

[1]Department of Biomedical Engineering, College of Engineering, Peking University, No. 5 Yiheyuan Road, Haidian District, Beijing, 100871, China, [2]Institute of Sports Medicine, Peking University Third Hospital, 49 North Garden Road, Haidian District, Beijing, 100191, China.

Rare-earth Yb^{3+} and Ho^{3+} co-doped fluorapatite (FA:Yb^{3+}/Ho^{3+}) crystals were prepared by hydrothermal synthesis, and their structure, upconversion properties, cell proliferation and imaging were investigated. The synthesized crystals, with a size of 16 by 286 nm, have a hexagonal crystal structure of classic FA and a Ca/Yb/Ho molar ratio of 100/16/2.1. Several reasonable Yb^{3+}/Ho^{3+} -embedding lattice models along the fluorine channel of the FA crystal cell are proposed for the first time, such as models for $(Ca_7YbHo©)(PO_4)_6F_2$ and $(Ca_6YbHoNa_2)(PO_4)_6F_2$. The activated FA:$Yb^{3+}/Ho^{3+}$ crystals were found to exhibit distinct upconversion fluorescence. The 543- and 654-nm signals in the emission spectra could be assigned, respectively, to the $^5F_4$ ($^5S_2$) - $^5I_8$ and $^5F_5$ - $^5I_8$ transitions of holmium via 980-nm near-infrared excitation and the energy transfer of ytterbium. After the surfaces were grafted with hydrophilic dextran, the crystals displayed clear fluorescent cell imaging. Thus, the prepared novel FA:Yb^{3+}/Ho^{3+} upconversion fluorescent crystals have potential applications in the biomedical field.

Some lanthanide ion-doped materials emit visible fluorescence when excited by a near-infrared (NIR) laser[1,2]. Typically, the sensitizers (usually Yb^{3+}) successively absorb NIR excitation over a range of 700–1000 nm and transfer the energy to the activators (Ho^{3+}, Er^{3+}, Tm^{3+}, etc.), followed by short-wavelength emission[3–6]. Compared to organic luminophores and semiconductor quantum dots (QDs)[7,8], these upconversion particles (UCPs) have advantages such as photostability, a sharp visible emission bandwidth, and nontoxicity[2,9]. For long-term bioimaging and cell-tracking studies, UCPs are preferable to organic luminophores, which are subject to photobleaching and display short excited state lifetimes, or QDs, which are potentially toxic in the cases of cadmium and selenium and display photoblinking and short circulation half-times[10,11]. In addition, in contrast to conventional downconversion fluorescent labels requiring an ultraviolet or blue excitation wavelength, UCPs show deep penetration in tissues, multiplexing ability, and the avoidance of tissue auto-fluorescence and possible fatal photodamage to cells[8,12]. Thus, UCPs are ideal fluorescent probes for a variety of biological applications, e.g., detection[13,14], imaging[15,16], cell tracking[17], and therapy[18]. Popular host matrixes that can house rare-earth ions to trigger upconverting fluorescence include $NaYF_4$[15], $NaGdF_4$[19], and $LaPO_4$[20]; however, their composition is not similar to that of biological apatite, which may block further *in vivo* biomedical applications. Herein, we selected an apatite matrix that can not only house lanthanide ions but also exhibit good biocompatibility and facilitate tissue-material interactions. Apatite crystals, including hydroxyapatite [$Ca_{10}(PO_4)_6(OH)_2$, HA] and fluorapatite [$Ca_{10}(PO_4)_6F_2$, FA], are often used as substitutes for the inorganic components of bones and teeth[21,22] due to their structural similarity to bone mineral, excellent biocompatibility, and bone-bonding bioactivity. Moreover, HA and FA can be employed as host materials for rare-earth doping as downconversion luminescent probes, such as in FA-Eu[23] and HA-Tb[24]. Lanthanide ions have a radius similar to that of Ca^{2+} ions and a high affinity to PO_4^{3-} ions[25,26], which can ensure the success of rare-earth doping. We chose FA as the doping matrix in this work because F^- ions can contribute materials with low phonon energies, which increase the number and probability of rare-earth luminescence transitions[22]. Although a few types of UCPs have been reported[11,16,27], there have been few studies on upconversion luminescence based on an FA matrix. The combination of the upconversion fluorescent properties of Yb/Ho ions with the excellent biocompatibility and typical crystal structure of FA allows us to design

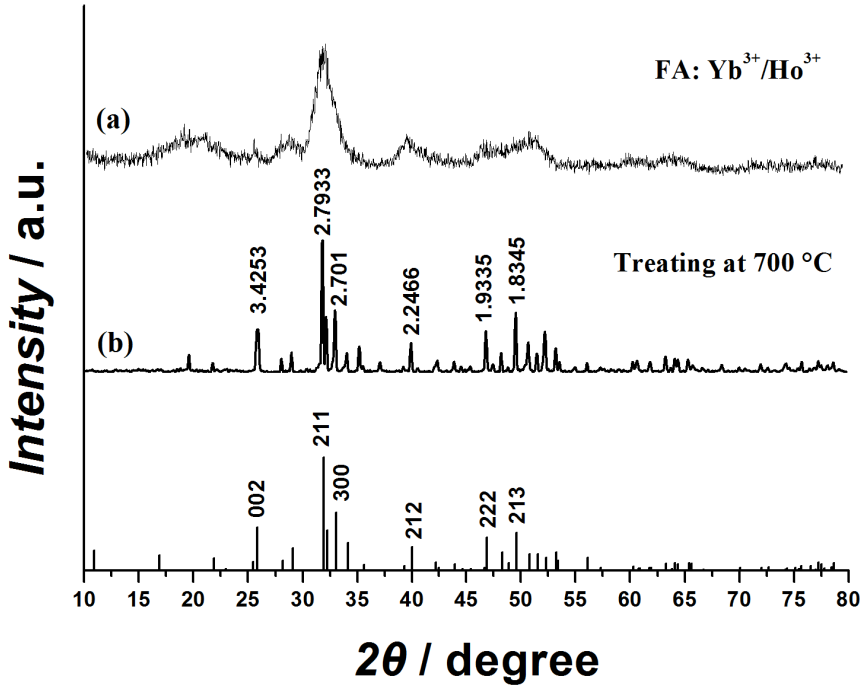

Figure 1 | XRD patterns of FA:Yb^{3+}/Ho^{3+} crystals after hydrothermal synthesis at 160°C for 16 h (a) and activation at 700°C for 2 h (b).

a promising material for biomedical applications. FA-based crystals have a high crystal stability due to their hexagonal structure and the presence of F^- ions. Thus, an FA matrix and Yb^{3+}/Ho^{3+} doping ions were chosen to synthesize FA:Yb^{3+}/Ho^{3+} crystals, and the possibility of upconversion fluorescence was investigated. In addition, bone marrow mesenchymal stem cells (BMSCs), which have shown great potential in tissue engineering[11,18,28], were employed to investigate the cell imaging and tracking abilities of the FA:Yb^{3+}/Ho^{3+} crystals.

In this work, we report the preparation and characterization of FA:Yb^{3+}/Ho^{3+} upconversion crystals. These rare-earth co-doped crystals were synthesized by a modified hydrothermal method[29,30], followed by activating treatment at 700°C. When excited under 980-nm NIR light, these crystals emit bright green (543 nm) and red (654 nm) light, possibly due to a mechanism of excited state absorption (ESA) and energy transfer (ET). After the surfaces were grafted with hydrophilic dextran, the crystals exhibited distinct cell fluorescence imaging.

Results and discussion

Figure 1 shows the XRD patterns of the FA:Yb^{3+}/Ho^{3+} crystals after hydrothermal synthesis at 160°C (a) and activation at 700°C (b). It is noted that Figure 1a shows only an envelope curve, indicating a poorly crystallized apatite structure. Figure 1b shows a much higher crystallinity than Figure 1a, with sharp characteristic peaks at 25.9° (002), 32° (211), 33.1° (300), 40.1° (212), and 46.7° (222), which match well with the classic hexagonal phase of $Ca_{10}(PO_4)_6F_2$ (JCPDS No. 77-0120) belonging to the $P6_3/m$ space group (176). The interplanar spacing of the [002] lattice plane is 3.42 Å or 0.342 nm. There are no impurity diffraction peaks or phases, such as those corresponding to rare-earth oxides, hydroxide, or fluoride, in the XRD patterns of the FA:Yb^{3+}/Ho^{3+} crystals, implying that the doping rare-earth ions were incorporated into the lattice of the fluorapatite crystals. The lattice parameters were determined by a least squares refinement using JADE software, with a = b = 0.938 nm, c = 0.688 nm for crystals synthesized at 160°C and a = b = 0.936 nm, c = 0.687 nm for crystals treated at 700°C, which both are in accord with the FA standard card (a = b = 0.937, c = 0.688 nm). However, the lattice parameters (a and c) of the crystals treated at 700°C are slightly smaller than those of the crystals synthesized at 160°C. This result indicates that the treatment at 700°C makes the crystal structure more dense due to recrystallization. The hexagonal crystal structure of fluorapatite has good crystal stability, which would be helpful for stable fluorescence expression of the embedded rare-earth ions.

Theoretically, we synthesized the rare-earth doped FA:Yb^{3+}/Ho^{3+} crystals according to a molar ratio of $X_{Ca}/Y_{Yb}/Z_{Ho}$ = 100/20/2 in the design formula of $(Ca_xYb_yHo_z)(PO_4)_6F_2$, through the reactions of $Ca(NO_3)_2$, $Yb(NO_3)_3$, $Ho(NO_3)_3$, Na_3PO_4, and NaF. Analytical data from the ICP-OES and SEM-EDS analyses (Table 1) illustrate that both Yb and Ho ions are incorporated into the FA crystals, and the measured molar ratio of $X_{Ca}/Y_{Yb}/Z_{Ho}$ in the synthesized FA:Yb^{3+}/Ho^{3+} crystals was found to be 100/16/2.1 by ICP-OES or 100/17/2.2 by EDS. The molar content of Yb ions is slight lower than the theoretical value, while the content of Ho ions is close to the theoretical value. Basically, the molar ratio of Ca/Yb/Ho is in accord with the theoretical ratio. After doping with Yb^{3+} and Ho^{3+} ions, the binding energies of Ca, P, and O in the doped FA crystals display a slight increase, as shown in the XPS data in Table 2. This trend indicates that the substitution of Yb^{3+} and Ho^{3+} ions for Ca^{2+} ions changes both the lattice parameters and the binding energy. This increase in binding energy suggests a stronger ion interaction in the doped apatite crystal structure.

It is known that the molecular formula of apatite or doped apatite is difficult to precisely replicate, especially when trivalent rare-earth

Table 1 | The molar ratio of Ca, Yb, and Ho in FA:Yb^{3+}/Ho^{3+} crystals via ICP-OES and SEM-EDS

	SEM-EDS (mol %)	ICP-OES (mol %)	Theoretical Value (mol %)
Ca/Yb/Ho	100/17/2.2	100/16/2.1	100/20/2

Table 2 | The binding energy of ions in FA:Yb^{3+}/Ho^{3+} crystals

	FA (eV)	FA:Yb^{3+}/Ho^{3+} (eV)
Ca (2p)	346.8	346.9
P (2p)	132.8	132.9
O (1s)	530.7	530.8

ions replace divalent calcium ions. If the molar ratio of Ca/Yb/Ho = 100/16/2.1 is used to calculate the molecular formula of the FA:Yb^{3+}/Ho^{3+} crystals, we obtain $(Ca_{8.5}Yb_{1.3}Ho_{0.2})(PO_4)_6F_2$; namely, in 10 crystal cells of FA:Yb^{3+}/Ho^{3+}, there are approximately 13 Yb^{3+} ions and 2 Ho^{3+} ions. Hence, each unit cell contains at least one Yb^{3+} ion, but only two unit cells contain both Yb^{3+} and Ho^{3+} ions. However, we will find a mismatch in the total valence in the formula $(Ca_{8.5}Yb_{1.3}Ho_{0.2})(PO_4)_6F_2$ when compared to $(Ca_{10})(PO_4)_6F_2$ of FA. For the balance of positive and negative valence, some Ca^{2+} vacancies or substitutions of O^{2-} for F^- should be present[31]. Moreover, a small number of monovalent sodium ions may exist to compensate for the valence mismatch. Indeed, Na^+ ions (Na 1s, 1070.8 eV) were found by the XPS analysis. Therefore, the substitution of Yb^{3+} or Ho^{3+} ions for Ca^{2+} ions in fluorapatite crystals should result in several different situations. The lattice occupation of Yb^{3+} and Ho^{3+} ions in 10 crystal cells can be divided into three situations: 1) one Yb^{3+} ion replaces one Ca^{2+} ion in each of five unit cells; 2) two Yb^{3+} ions replace two Ca^{2+} ions in each of three unit cells; and 3) one Yb^{3+} ion and one Ho^{3+} ion replace two Ca^{2+} ions in each of two unit cells. For the first situation, a reasonable valence-balanced formula is $(Ca_9Yb)(PO_4)_6FO$, or $(Ca_8YbNa)(PO_4)_6F_2$; for the second situation, the balanced formula could be $(Ca_7Yb_2©)(PO_4)_6F_2$ (©-Ca vacancy) or $(Ca_6Yb_2Na_2)(PO_4)_6F_2$; for the third situation, a reasonable balanced formula is $(Ca_7YbHo©)(PO_4)_6F_2$ (©-Ca vacancy) or $(Ca_6YbHoNa_2)(PO_4)_6F_2$. Figure 2 displays a schematic diagram for the three situations of Yb/Ho-embedding lattice models along the fluorine channel of an FA crystal cell.

We further investigated the crystal morphology and structure by transmission electron microscopy (TEM) combined with energy dispersive spectroscopy (EDS), high-resolution (HRTEM) imaging, and selected area electron diffraction (SAED) (Figure 3). As shown in Figure 3a, the FA:Yb^{3+}/Ho^{3+} crystals after hydrothermal synthesis at 160°C exhibit a fusiform morphology, with an average crystal size of approximately 26 nm by 250 nm. After activation treatment at 700°C, these crystals still exhibit a slender shape with an average size of 16 nm by 286 nm (Figure 3b). The average center diameter of the nanocrystals decreases to 16 nm from 26 nm (a decrease of approximately 38%) while the average length increases to 286 nm from 250 nm (an increase of approximately 14%). This behavior indicates that recrystallization occurs during the heating process, which agrees well with the enhanced crystallinity shown in Figure 1b. Figure 3c provides a TEM-EDS element mapping of the crystals, demonstrating the successful incorporation of Yb^{3+} and Ho^{3+} ions in the crystal structure. Figure 3d displays a HRTEM image showing the presence of 2D lattice fringes for a single slender FA:Yb^{3+}/Ho^{3+} crystal. The crystal shows preferential growth along the [002] direction, and the interplanar spacing of the [002] lattice plane is 0.346 nm, in accord with the results (0.342 nm) from XRD analysis. Figure 3d also shows an inset of SAED pattern for the (002), (212), and (211) planes, which are in good agreement with the XRD pattern. The results confirm that the slender crystals exhibit a typical single crystal structure with uniform morphology and good crystallinity. The good dispersity and narrow size distribution of these crystals are expected to arise from the surfactant intervention during hydrothermal synthesis, the freeze-drying process, and the relatively lower activation temperature compared to previous studies conducted at 900°C[20].

The activating treatment of rare-earth co-doped material is important for acquiring stable upconversion emission. We chose 700°C for our treatment of Yb^{3+}/Ho^{3+} co-doped apatite nanocrystals because it was found that at this temperature, the FA:Yb^{3+}/Ho^{3+} nanocrystals exhibited an obvious upconversion emission while maintaining good dispersity. For treatment at temperatures under 650°C, almost no apparent upconversion emission was present.

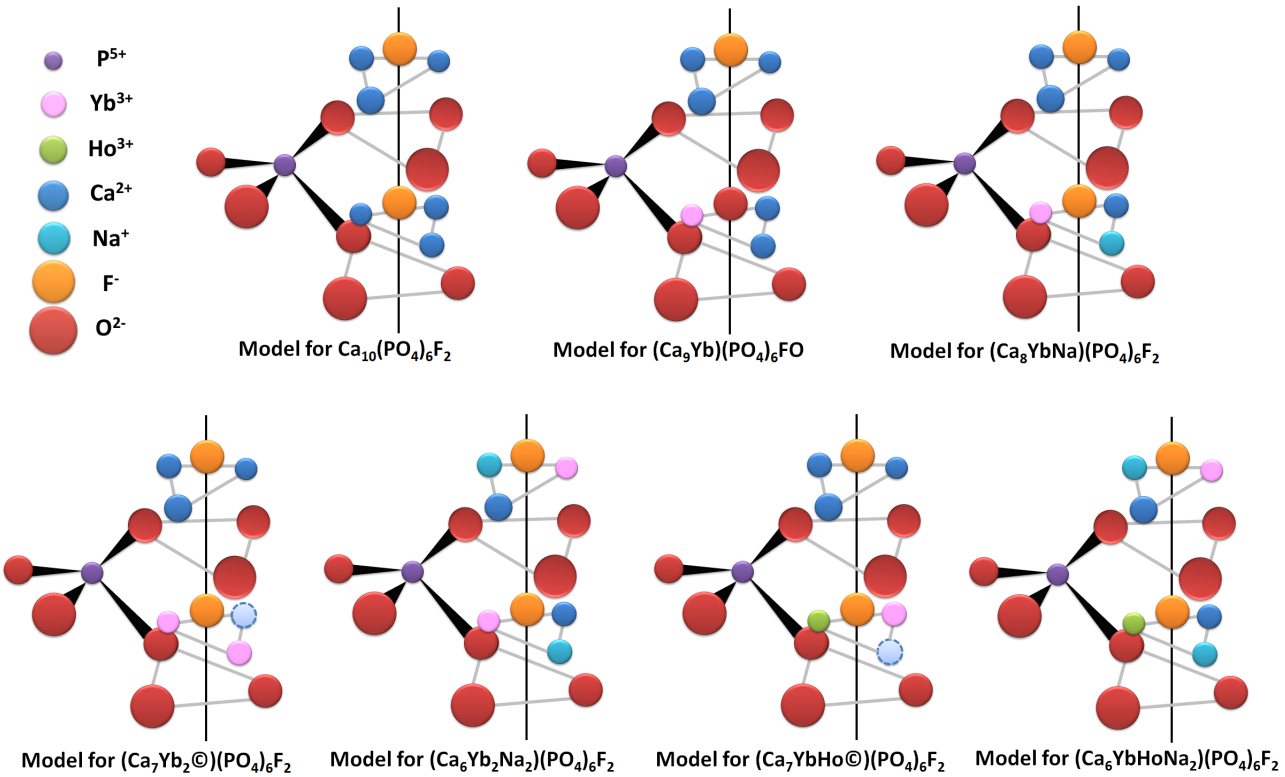

Figure 2 | Schematic diagram of a Yb/Ho-embedding lattice model along the fluorine channel of FA crystal cell.

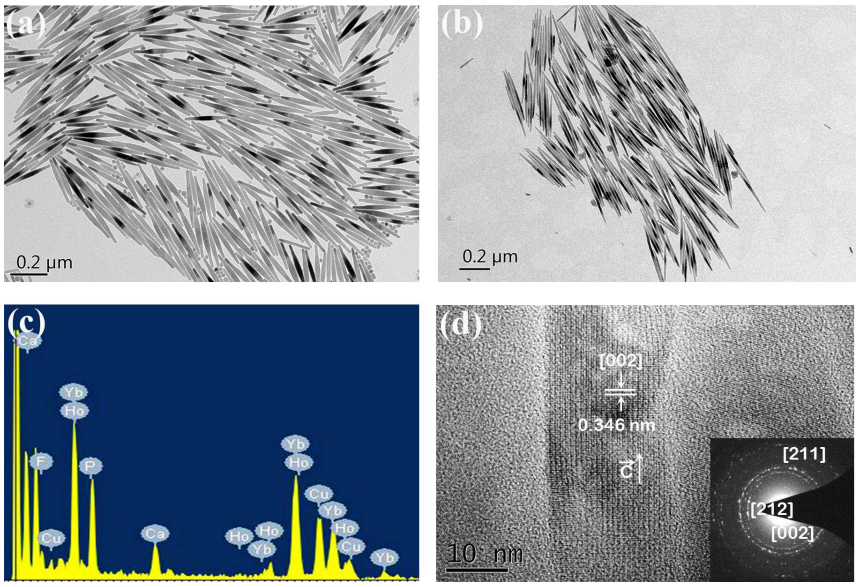

Figure 3 | **TEM micrographs of FA:Yb^{3+}/Ho^{3+} crystals after hydrothermal synthesis at 160 °C (a) and activation at 700 °C (b), element mapping by EDS (c), and HRTEM imaging of a single FA:Yb^{3+}/Ho^{3+} crystal with an inset showing the SAED pattern (d).**

Above 750°C, the nanocrystals melted and fused together to form a ceramic state. Thus, treatment at 700°C enhances the crystallinity and structure stability of the FA:Yb^{3+}/Ho^{3+} crystals, which especially promotes the upconversion effect. When excited by 980-nm NIR light, the Yb^{3+}/Ho^{3+} co-doped crystals chiefly display two fluorescence emission bands, namely, a green band centered at 543 nm and a red band near 654 nm, while the crystals that were not activated at 700°C do not exhibit any obvious emission (Figure 4a). The 491-nm emission should be attributed to the 980-nm laser. To determine the number of photons (n) involved in the upconversion process, the pump power dependence of the luminescence intensity was investigated, as shown in Figure 4b. The slope (n) values are 2.0 for both the green and red emission bands, demonstrating that a two-photon absorption process is involved in the upconversion emission.

Although a few Yb^{3+}/Ho^{3+} co-doped upconversion materials have been reported[32,33], biocompatible fluorapatite was used in this experiment solely as a matrix for UCPs, and thus, the upconversion mechanism needs further exploration. Here, we speculate a mechanism for the upconversion process of the FA:Yb^{3+}/Ho^{3+} crystals upon NIR excitation at 980 nm (Figure 5). In the crystal lattice of FA, some Ca^{2+} sites are occupied by Yb^{3+} and Ho^{3+} ions. Because the content of Yb^{3+} ions is much higher than that of Ho^{3+} ions, each Ho^{3+} ion is surrounded by several Yb^{3+} ions in the FA crystal. First, the sensitizer Yb^{3+} ions are excited from the $^2F_{7/2}$ to $^2F_{5/2}$ level upon the absorption of NIR photons (980 nm). The ions then transfer energy to the adjacent activator Ho^{3+} ions, exciting the ground Ho^{3+} ions to the $^5I_6$ level. For green emission, Ho^{3+} ions at the $^5I_6$ level can be directly excited to the $^5F_4$, $^5S_2$ level by absorbing energy from the laser photons (excited state absorption, ESA)[27]. For red emission, the Ho^{3+} ions at the $^5I_6$ level can drop to the $^5I_7$ level via nonradioactive phonon-assisted relaxation; they can then be excited to the $^5F_5$ level by absorbing energy from the laser photons. The radioactive transfer of the Ho^{3+} ($^5F_4$, $^5S_2$) and Ho^{3+} ($^5F_5$) ions to the ground state results in green emission centered at 543 nm and red emission centered at 654 nm, respectively. The Yb^{3+} ions surrounding the Ho^{3+} ions are helpful for facilitating excitation energy transfer and are also separated by a considerable number of optically inactive Ca^{2+} ions to avoid energy migration to capture traps.

The proliferation of cells cultured with different dosages of FA:Yb^{3+}/Ho^{3+} crystals was evaluated using a cell counting kit-8

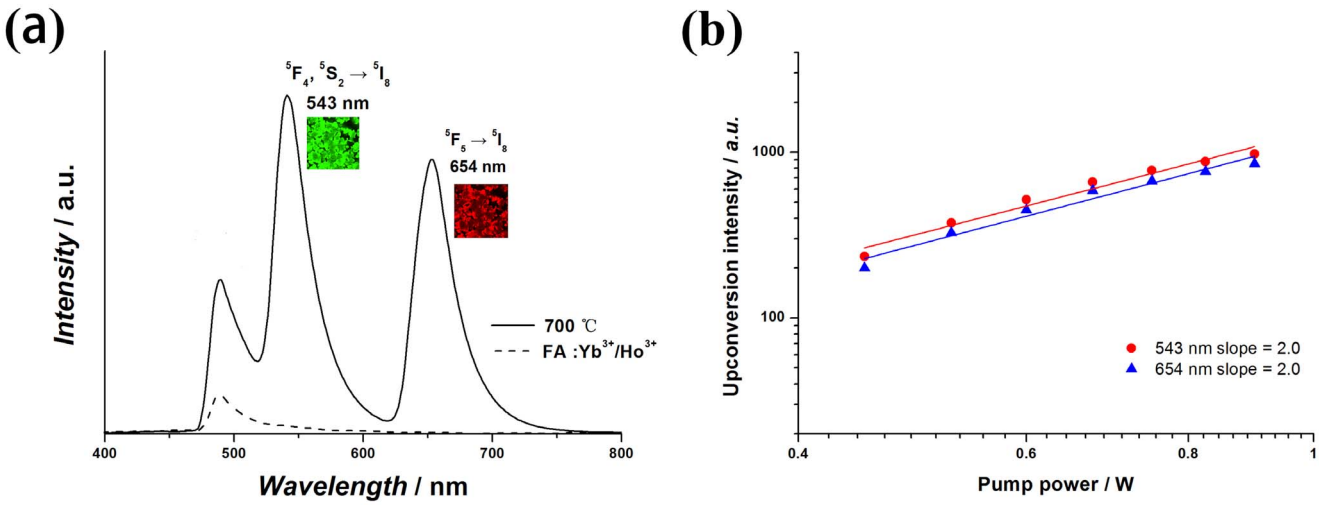

Figure 4 | Upconversion emission spectra (a) of FA:Yb^{3+}/Ho^{3+} crystals with (solid curve) and without (dashed curve) activation at 700°C, with the insets showing laser confocal images. Dependence of the upconversion emission intensity on the NIR pump power (b).

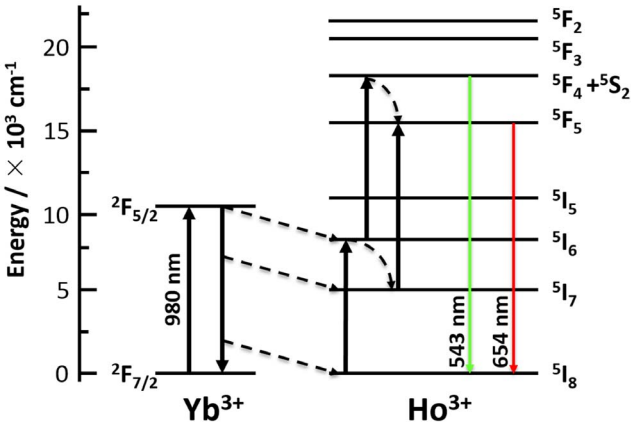

Figure 5 | Schematic energy-level diagram of Ho^{3+} and Yb^{3+} ions and the upconversion luminescence mechanism for FA:Yb^{3+}/Ho^{3+} crystals.

(CCK-8) assay. Figure 6 shows that the cell proliferation for different dosage groups increases markedly and continuously with time, showing a normal growth trend, even at a high dosage of 800 μg mL^{-1}. On Day 1, all experimental groups show proliferation comparable to the control ($\rho > 0.05$). On Day 3, although the cell proliferation for the 100- and 200-μg mL^{-1} dosage groups is lower than that of the control and the 400- and 800-μg mL^{-1} dosage groups ($\rho < 0.05$), they still exhibit a normal growth status. This result indicates that the cytotoxicity of the rare-earth doped crystals is tolerable, allowing for further studies of live-cell imaging.

To explore the potential of FA:Yb^{3+}/Ho^{3+} crystals for future biomedical applications, we used hydrophilic dextran to graft the surface of these crystals for cell imaging. Figure 7 shows the IR spectra of the FA:Yb^{3+}/Ho^{3+} crystals treated at 700°C, the dextran and dextran-grafted FA:Yb^{3+}/Ho^{3+} crystals. The absorption peaks at 3411 and 1652 cm^{-1} in Figure 7c attribute to the typical stretching vibration and bending vibration of the -OH groups, and the absorption peak at 2930 cm^{-1} is the typical stretching vibration of C-H in dextran. By comparing Figure 7c with Figure 7b, the presence of $-CH_2$ and -OH peaks and the peak shift (e.g., from 2926 to 2930 cm^{-1} for $-CH_2$ groups) provide evidence of successful grafting of hydrophilic dextran on the crystals. The peak shift should be caused by the bonding or interaction between the crystals and dextran. Other peaks at 1043 and 960 cm^{-1} (asymmetrical stretching vibration) and 606 and 575 cm^{-1} (bending vibration) correspond to the PO_4^{3-} groups, similar to the FA:Yb^{3+}/Ho^{3+} crystals without a grafting (Figure 7a). The dextran-grafted FA:Yb^{3+}/Ho^{3+} crystals are small in size and exhibit distinct upconversion fluorescence, good cytocompatibility, and crystal stability, making them suitable for bioimaging investigation.

A combination of 100-μg mL^{-1} dextran-grafted FA:Yb^{3+}/Ho^{3+} crystals and BMSCs was used to investigate the possibility of cell imaging. The results of *in vitro* cell imaging demonstrate the cellular uptake of the crystals, as shown in Figure 8. When BMSCs treated with these crystals were exposed to 980-nm excitation, the cells showed strong cellular upconversion fluorescence. The cell morphology and cytoplasm can be clearly observed. The green (a) and red (b) fluorescent images of the cells match well with the bright-field image of the cells (c) and provide clear overlap images (d). Moreover, the upconversion luminescence of the FA:Yb^{3+}/Ho^{3+} crystals is stable and reproducible; the samples maintained reproducibility after 7 days. This result indicates the feasibility of using these upconversion crystals for cell imaging and tracking via their easy translocation into the cytoplasm of cells. Furthermore, the optical absorption of cellular components under NIR excitation is much lower than that for UV or visible light, which is helpful for reducing photodamage and for improving the sensitivity due to the absence of auto-fluorescence[28]. These features can also pave the way for imaging and tracking cells with multilineage differentiation.

In addition to cell imaging, the Yb^{3+}/Ho^{3+} co-doped apatite nanocrystals will have broad applications in biomedical fields. Using the good biocompatibility, bone-bonding bioactivity, and upconversion fluorescence of these rare-earth doped apatite nanocrystals, we can produce porous composite scaffolds with biodegradable polymers to investigate the process of bone repair and regeneration, determine whether synthetic apatite nanocrystals can incorporate into newly formed bone, reveal the bone-biomaterial interface via fluorescent imaging, trace the degradation of scaffolds, distinguish the scaffold material from bone tissue in histological sections, etc. Therefore, investigations on the upconversion properties of such Yb^{3+}/Ho^{3+} co-doped apatite nanocrystals have significance in scientific studies and biomedical applications.

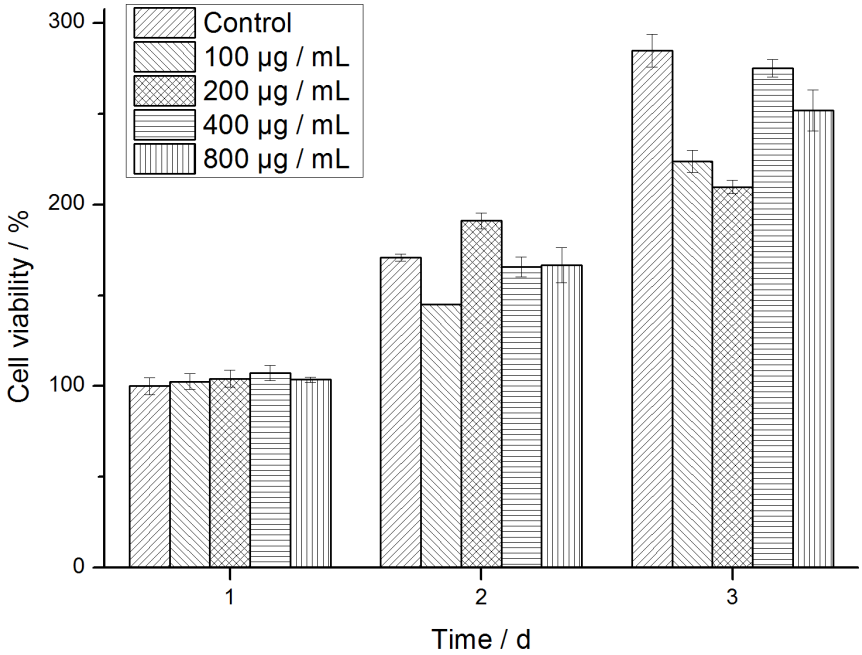

Figure 6 | CCK-8 assay of cell proliferation after cell culture with different dosages of FA:Yb^{3+}/Ho^{3+} crystals for 1, 2, and 3 days.

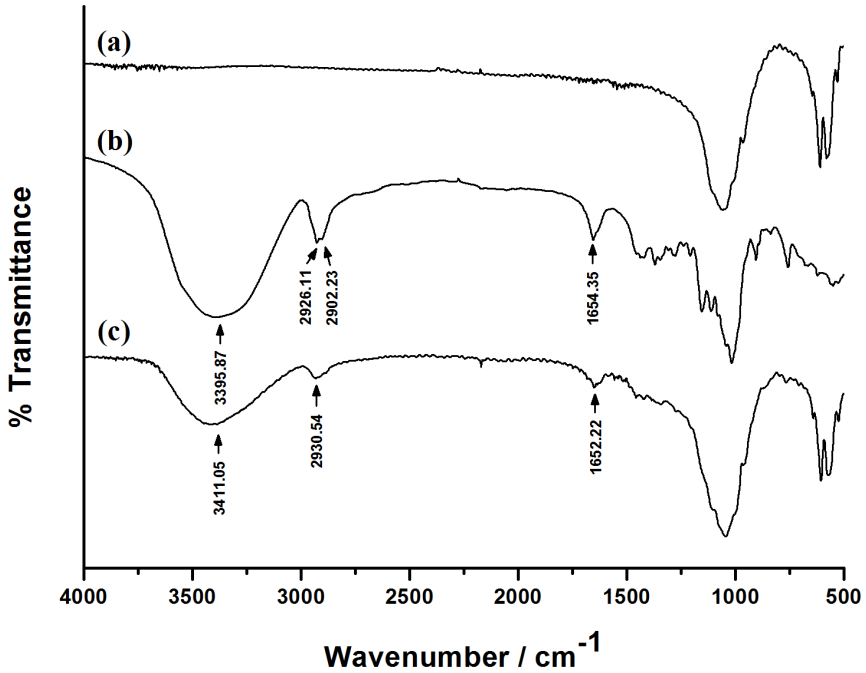

Figure 7 | FTIR spectra of the FA:Yb^{3+}/Ho^{3+} crystals treated at 700°C (a), dextran (b) and dextran-grafted FA:Yb^{3+}/Ho^{3+} crystals (c).

Methods

Materials. $Ca(NO_3)_2{\cdot}4H_2O$, $Yb(NO_3)_3{\cdot}5H_2O$, $Ho(NO_3)_3{\cdot}5H_2O$, $Na_3PO_4{\cdot}12H_2O$, NaF, octadecylamine, oleic acid, ethanol, and cyclohexane at AR grade were obtained from Beijing Chemical Reagents Company, China. Dextran 20,000 at AR grade was purchased from Sinopharm Chemical Reagent Company, China. All other chemical agents obtained from commercial routes were of analytical grade and were used without further purification.

Preparation of FA:Yb^{3+}/Ho^{3+} crystals. Octadecylamine (0.5 g) was dissolved in oleic acid (4 mL) and ethanol (16 mL) under magnetic stirring in a Teflon-lined autoclave (50 mL). Then, an aqueous solution of $Ca(NO_3)_2$ (0.28 M, 7 mL), $Ln(NO_3)_3$ (Ln: 0.20 M Yb^{3+} + 0.02 M Ho^{3+}, 2 mL), Na_3PO_4 (0.20 M, 7 mL), and NaF (0.24 M, 2 mL) was added. Afterwards, the mixture was agitated for 10 min and hydrothermally treated at 160°C for 16 h. After cooling to room temperature naturally, a white precipitate was collected by centrifugation (10 min at 2700 × g), washed, and activated at 700°C in air for 2 h at a heating rate of 1°C/min.

Dextran grafting of FA:Yb^{3+}/Ho^{3+} crystals. The prepared rare-earth doped crystals (0.5 g) were added to a dextran solution (1 g, 7 mL) in a 10-mL round-bottom flask. The mixture was dispersed by ultrasonication and stirred for 2 h at room temperature to obtain a homogeneous phase. Then, the crystals were isolated by centrifugation (3 min at 4000 × g) and purified with distilled water and ethanol three times. We verified that the product could be re-dispersed in an aqueous solution.

Characterization. X-ray powder diffraction (XRD) patterns were acquired with a Philips X′ Pert Pro MPD apparatus over a 2θ range of 10° to 80° using Cu Kα radiation (λ = 1.5406 Å). TEM images of the crystals were collected on an FEI TecnaiG2 T20 instrument at 200 kV. Energy dispersive spectroscopy (EDS) data were obtained by both TEM and scanning electron microscopy (SEM, JEOL, JSM-5900LV). ICP-OES measurements were conducted on a Prodigy ICP-OES (Teledyne Leeman Labs), and each data point was expressed as the mean ± SD based on triplicate dishes. The binding energy data were measured as an XPS spectrum, AXIS Ultra DLD, Kratos, UK. Fourier transform infrared spectra (FTIR) were recorded on a Perkin-Elmer 6000 Fourier transformation spectrometer, with a wavenumber range of 400–4000 cm^{-1}. The photoluminescence behavior was recorded using a Hitachi F-7000 fluorescence spectrophotometer with an external 0- to 2-W adjustable diode laser integrated with an optical fiber (Beijing Hi-Tech Optoelectronic Co., China).

Cytotoxicity assay. HeLa cells provided by the Institute of Sports Medicine, Peking University Third Hospital, China were used for the cytotoxicity assay. The cells were seeded in a 96-well flat-bottomed microplate (5000 cells/well) and cultured in 100 μL of growth medium at 37°C and 5% CO_2 for 24 h. The cell culture medium in each well was then replaced with 100 μL of cell growth medium containing FA:Yb^{3+}/Ho^{3+} crystals at concentrations of 100, 200, 400, and 800 μg mL^{-1}. After incubation for 1, 2, and 3 days at 37°C, the crystals were washed with PBS three times. Then, 10 μL of CCK-8 dye and 100 μL of α-MEM cell culture medium were added to each well, and the cells were incubated for another 3 h at 37°C. The absorbance at 450 nm was measured by a Varioskan Flash instrument (Thermo Scientific), and the results are presented as the mean ± SD from triplicate wells. A value of $\rho < 0.05$ was considered to be statistically significant.

Upconversion bioimaging. BMSCs were provided by the Institute of Sports Medicine, Peking University Third Hospital, China. The cells were grown in α-MEM (Minimum Essential Medium, Alpha Modified) supplemented with 10% FBS (fetal bovine serum) and cultured at 37°C under 5% CO_2. The BMSCs were seeded onto 35-mm coverglass-bottom dishes and incubated in 2 mL of α-MEM at 37°C for 24 h. The culture medium was removed, and the cells were incubated in 2 mL of α-MEM containing FA:Yb^{3+}/Ho^{3+} crystals (100 μg mL^{-1}) at 37°C for 24 h. After being rinsed with PBS three times, the cells were fixed with 4% paraformaldehyde for 15 min. Upconversion fluorescence imaging was conducted under a multiphoton confocal microscope (Leica TCS SP8) at 980 nm. The green and red upconversion luminescence emission was collected at 540 ± 40 nm and 650 ± 40 nm, respectively.

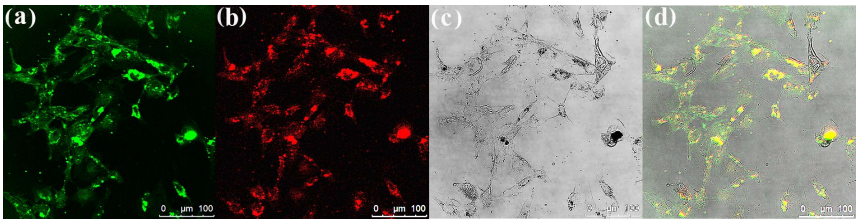

Figure 8 | Multiphoton confocal luminescence images (excited by 980-nm light) of BMSCs incubated with 100-μg mL^{-1} dextran-grafted FA:Yb^{3+}/Ho^{3+} crystals for 24 h at 37°C. The figures show green (a) and red (b) upconversion luminescence images of BMSCs, a bright-field image of the cells (c), and an overlay image (d) of green plus red. The green and red luminescence emission was collected at 540 ± 40 nm and 650 ± 40 nm, respectively.

Conclusion

A fluorapatite crystal matrix was chosen for the doping of Yb^{3+} and Ho^{3+} ions for the first time, which successfully resulted in upconversion luminescence. The substitution of Yb^{3+} and Ho^{3+} ions for Ca^{2+} ions changes both the lattice parameters and the binding energy. The proposed lattice models demonstrate the importance of the coexistence of different lattice substitutions of Yb^{3+} and Ho^{3+} ions in the FA crystal structure. When excited by 980-nm NIR light, the FA:Yb^{3+}/Ho^{3+} crystals display bright green and red emission with narrow emission bands at 543 and 654 nm, respectively. When the surfaces are grafted with hydrophilic dextran, the crystals exhibit distinct cell fluorescent imaging by entering the cytoplasm of cells. These rare-earth doped crystals with good cytocompatibility, a stable crystal structure, fluorescent repeatability, and bioactivity show great potential for biomedical applications.

1. Auzel, F. Upconversion and anti-stokes processes with f and d ions in solids. *Chem. Rev.* **104**, 139–174 (2003).
2. Wang, F. *et al.* Simultaneous phase and size control of upconversion nanocrystals through lanthanide doping. *Nature* **463**, 1061–1065 (2010).
3. Mullen, T. J. *et al.* Fabrication and characterization of rare-earth-doped nanostructures on surfaces. *ACS Nano* **5**, 6539–6545 (2011).
4. Chen, Z. *et al.* Versatile synthesis strategy for carboxylic acid−functionalized upconverting nanophosphors as biological labels. *J. Amer. Chem. Soc.* **130**, 3023–3029 (2008).
5. Yi, G., Peng, Y. & Gao, Z. Strong red-emitting near-infrared-to-visible upconversion fluorescent aanoparticles. *Chem. Mater.* **23**, 2729–2734 (2011).
6. Zhou, J., Liu, Z. & Li, F. Upconversion nanophosphors for small-animal imaging. *Chem. Soc. Rev.* **41**, 1323–1349 (2012).
7. Bünzli, J.-C. G. Lanthanide luminescence for biomedical analyses and imaging. *Chem. Rev.* **110**, 2729–2755 (2010).
8. Larson, D. R. *et al.* Water-soluble quantum dots for multiphoton fluorescence imaging in vivo. *Science* **300**, 1434–1436 (2003).
9. Idris, N. M. *et al.* Tracking transplanted cells in live animal using upconversion fluorescent nanoparticles. *Biomaterials* **30**, 5104–5113 (2009).
10. Nam, S. H. *et al.* Long-term real-time tracking of lanthanide ion doped upconverting nanoparticles in living cells. *Angew. Chem. Int. Ed.* **50**, 6093–6097 (2011).
11. Goldmacher, G. V. *et al.* Tracking transplanted bone marrow stem cells and their effects in the rat MCAO stroke model. *PLoS ONE* **8**, e60049 (2013).
12. Li, Z. & Zhang, Y. Monodisperse silica-grafted polyvinylpyrrolidone/$NaYF_4$ nanocrystals with multicolor upconversion fluorescence emission. *Angew. Chem. Int. Ed.* **45**, 7732–7735 (2006).
13. Liu, Q., Peng, J., Sun, L. & Li, F. High-efficiency upconversion luminescent sensing and bioimaging of Hg(II) by chromophoric ruthenium complex-assembled nanophosphors. *ACS Nano* **5**, 8040–8048 (2011).
14. Liu, Y. *et al.* A Cyanine-modified nanosystem for in vivo upconversion luminescence bioimaging of methylmercury. *J. Amer. Chem. Soc.* **135**, 9869–9876 (2013).
15. Jin, J. *et al.* Polymer-grafted $NaYF_4$:Yb^{3+}, Er^{3+} upconversion nanoparticles for charge-dependent cellular imaging. *ACS Nano* **5**, 7838–7847 (2011).
16. Wang, Y.-F. *et al.* Nd^{3+}-sensitized upconversion nanophosphors: efficient in vivo bioimaging probes with minimized heating effect. *ACS Nano* **7**, 7200–7206 (2013).
17. Zhou, A. *et al.* Pyropheophorbide a and c(RGDyK) comodified chitosan-wrapped upconversion nanoparticle for targeted near-infrared photodynamic therapy. *Mol. Pharmaceutics* **9**, 1580–1589 (2012).
18. Osanai, T. *et al.* Therapeutic effects of intra-arterial delivery of bone marrow stromal cells in traumatic brain injury of rats—in vivo cell tracking study by near-infrared fluorescence imaging. *Neurosurgery* **70**, 435–44 (2012).
19. Vetrone, F. *et al.* The active-core/active-shell approach: a strategy to enhance the upconversion luminescence in lanthanide-doped nanoparticles. *Adv. Funct. Mater.* **19**, 2924–2929 (2009).
20. Ghosh, P. *et al.* Enhancement of upconversion emission of $LaPO_4$:Er@Yb core−shell nanoparticles/nanorods. *J. Phys. Chem. C* **112**, 9650–9658 (2008).
21. Chen, H. *et al.* Interaction of dendrimers (artificial proteins) with biological hydroxyapatite crystals. *J. Dent. Res.* **82**, 443–448 (2003).
22. Chen, H. *et al.* Synthesis of fluorapatite nanorods and nanowires by direct precipitation from solution. *Crys. Grow. Des.* **6**, 1504–8 (2006).
23. Sun, Y., Yang, H. & Tao, D. Preparation and characterization of Eu^{3+}-doped fluorapatite nanoparticles by a hydrothermal method. *Ceramics International* **38**, 6937–6941 (2012).
24. Yang, C. *et al.* Solvothermal synthesis and characterization of Ln (Eu^{3+}, Tb^{3+}) doped hydroxyapatite. *J. Colloid Interface Sci.* **328**, 203–210 (2008).
25. Huang, C. H. *Coordination Chemistry of Rare Earth Complexes.* (Science Press, Beijing, 1997).
26. Hui, J. & Wang, X. Luminescent, colloidal, F-substituted, hydroxyapatite nanocrystals. *Chem. Euro. J.* **17**, 6926–6930 (2011).
27. Lai, B. *et al.* Multi-phonon-assisted relaxation and Yb^{3+} sensitized bright red-dominant upconversion luminescence of Ho^{3+} in YF_3-BaF_2-$Ba(PO_3)_2$ glass. *Appl. Phys. B* **110**, 101–110 (2013).
28. Wang, C., Cheng, L., Xu, H. & Liu, Z. Towards whole-body imaging at the single cell level using ultra-sensitive stem cell labeling with oligo-arginine modified upconversion nanoparticles. *Biomaterials* **33**, 4872–4881 (2012).
29. Hui, J. *et al.* Fluoridated HAp:Ln^{3+} (Ln = Eu or Tb) nanoparticles for cell-imaging. *Nanoscale* **4**, 6967–6970 (2012).
30. Wang, X., Zhuang, J., Peng, Q. & Li, Y. A general strategy for nanocrystal synthesis. *Nature* **437**, 121–124 (2005).
31. Ternane, R., Trabelsi-Ayedi, M., Kbir-Ariguib, N. & Piriou, B. Luminescent properties of Eu^{3+} in calcium hydroxyapatite. *J. Lumin.* **81**, 165–170 (1999).
32. Zhang, X. X., Hong, P., Bass, M. & Chai, B. H. T. Ho^{3+} to Yb^{3+} back transfer and thermal quenching of upconversion green emission in fluoride crystals. *Appl. Phys. Lett.* **63**, 2606–2608 (1993).
33. Sangeetha, N. M. & van Veggel, F. C. J. M. Lanthanum silicate and lanthanum zirconate nanoparticles co-doped with Ho^{3+} and Yb^{3+}: matrix-dependent red and green upconversion emissions. *J. Phys. Chem. C* **113**, 14702–14707 (2009).

Acknowledgments

The authors acknowledge support from Project (2012CB933903) from the National Basic Research Program of China.

Author contributions

H.C. and Y.A. developed the idea and supervised the project. X.L. conducted most of the experiments, and J.Z. and Z.M. helped with cell experiments. All authors discussed the results and contributed to writing the manuscript.

Additional information

Competing financial interests: The authors declare no competing financial interests.

How to cite this article: Li, X.Y., Zhu, J.X., Man, Z.T., Ao, Y.F. & Chen, H.F. Investigation on the structure and upconversion fluorescence of Yb^{3+}/Ho^{3+} co-doped fluorapatite crystals for potential biomedical applications. *Sci. Rep.* **4**, 4446; DOI:10.1038/srep04446 (2014).